Proceedings of ASME Turbo Expo 2011
GT2011
June 6-10, 2011, Vancouver, British Columbia, Canada

GT2011-45920

CONJUGATE HEAT TRANSFER ANALYSIS OF A FILM-COOLED TURBINE VANE

Ron Ho Ni
William Humber
George Fan
AeroDynamic Solutions, Inc.
Pleasanton, California, 94566

P. Dean Johnson
Jim Downs
Florida Turbine Technologies, Inc.
Jupiter, Florida, 33458

J. P. Clark
P. J. Koch
Air Force Research Laboratory
Wright-Patterson AFB, OH, 45433

ABSTRACT

A conjugate heat transfer analysis methodology has been defined and applied to an Air Force film cooled turbine vane consisting of 648 cooling holes. An unstructured computational mesh was used to model both the fluid and metal sides of the turbine vane. A summary of the numerical methods employed by Code Leo is provided along with a description of the coupling procedure employed between the fluid and heat conduction computations. Numerical simulations were conducted at multiple mesh resolutions to assess accuracy and repeatability. A detailed review is presented for the numerical solution obtained from a fine mesh consisting of 24 million elements (8 million solid, 16 million fluid) covering all 648 film holes. Results showed that cooled air from the film holes formed a protective layer around the airfoil surfaces and endwalls as intended. Low metal temperatures were present not only on the external surfaces exposed to hot gas, but also around the entrances to the film cooling holes. Cooled air was also observed to pile up along the pressure surface at mid-span. Solution convergence was achieved in approximately 15,000 iterations and 100 hours elapsed time on a dual-socket Intel E5504 workstation. The combination of fast turnaround time with accurate metal temperature prediction will enable conjugate heat transfer analysis to be easily incorporated into routine design processes to better address durability goals.

NOMENCLATURE

P_t	Total Pressure
T_T	Total Temperature
P_S	Exit Static Pressure
q	Heat Flux
ID	Hub Surface of the Turbine Vane
OD	Shroud Surface of the Turbine Vane
1V	First Vane
1B	First Blade
2V	Second Vane
BOAS	Blade Outer Air Seal
s	Subscript for Solid
f	Subscript for Fluid

INTRODUCTION

The continuing quest for higher gas turbine performance and fuel efficiency has led to smaller, lighter engine designs capable of operating with heavy airfoil loadings at extremely high temperatures. These conditions pose a great challenge for designers seeking to meet demanding durability goals. Higher gas temperatures must be countered by efficient cooling schemes to mitigate adverse thermal loading on hot section components. Heavier time varying loads resulting from tighter axial gaps must be mitigated during design by better anticipating rotor-stator interaction effects. Without accounting for these thermal and aerodynamic loads, durability of next generation commercial and military gas turbine engines will be compromised.

Currently, the design practices employed by the major OEMs for cooled turbine airfoils are generally empirical in nature and can easily miss important physical behaviors impacting durability.

Company proprietary methods are typically used to establish the external and internal convective boundary conditions with inclusion of film cooling correlations. Metal temperatures in hot section components are then obtained by imposing convective boundary conditions on the external and internal (in the case of cooled turbine airfoils) surfaces of the part and then solving the conduction equations for the part itself. Vendor codes are most often utilized to execute the thermal conduction solution of the metal part to obtain the transient and steady state temperature fields and allow the computation of thermally-driven stresses in a component part.

In many cases, the external heat transfer coefficients are predicted employing boundary layer codes such as Stan5 or TexStan or by full 3D CFD computations. Some of these methods address film cooling directly in the computation; others apply empirical factors to the non-film cooled heat transfer coefficients. The internal heat transfer coefficients are often determined by employing heat transfer correlations based on data obtained in channel testing reflecting turbine airfoil cooling passages. These correlations are also used to make predictions of the effect of heat transfer augmentation devices.

These existing design methods can be best categorized as loosely coupled procedures based upon simplified approximation (2-D aero) and data correlation. They require the execution of multiple codes, with large amounts of data exchanged between these codes that can result in lower accuracy and greater potential for execution error.

In recent years, research efforts have focused on 3-D conjugate heat transfer analysis as a means to provide more accurate and reliable prediction of metal temperature of hot parts [1] [2] [3] [4] [5] [6]. This approach offers several key advantages:

- Better understanding of the flow around film cooling holes and its effect on metal temperature surrounding the holes and the heat transfer on the endwalls with film holes.
- A simpler and more streamlined procedure for turbine durability analysis.

By producing more reliable temperature field predictions for advanced turbine component parts, especially airfoils, OEMs gain the means to improve in-service durability performance.

A number of issues remain, however, before fully coupled, high fidelity CHT tools can be used routinely during design. They are: (1) good turbulence models for reliable flow and heat transfer predictions; (2) experimental data in a engine environment for code validation, and; (3) a simulation procedure that is easy to use and fast enough to fit within today's tight design windows. Much research has been devoted to issues associated with turbulence modeling and prediction validation; the major focus of this effort is to develop a CHT analysis capability that is both fast and reliable enough to allow engineers to assess its accuracy and advantages against a wide variety of turbine configurations.

This paper describes the CHT analysis capability developed for Code Leo and its application to a film cooled turbine vane. The test case will first be described, followed by the CHT analysis methodology and the numerical methods and coupling procedure employed for the CHT problem. A discussion of the numerical results obtained from its application to a film cooled turbine vane ensues, followed by concluding remarks.

CASE DESCRIPTION

The Air Force Research Laboratory (AFRL) has been heavily involved in design-code validation for a number of years. However, many of the efforts undertaken to date were restricted by proprietary considerations [7] [8]. In late 2002, the Scientific Advisory Board of the US Air Force recommended that the laboratory commit itself to turbine research that benefits the industry as a whole instead of a single company. Accordingly, it was recognized that non-proprietary geometries were a pre-requisite to such work. So, a suite of design tools was developed and implemented at the laboratory [9], and the High Impact Technologies Research Turbine (HIT RT) was created. The HIT RT is illustrated in figure 1. It is a stage-and-one-half high pressure turbine that is consistent with a dual-spool engine that has an Overall Pressure Ratio (OPR) of 40. The turbine stage is transonic with a design total-to-total pressure ratio of 3.75, a speed parameter of 361 $RPM \cdot K^{-1/2}$, $AN^2 = 3.7x10^7\ (m \cdot RPM)^2$, and a reaction based on static pressure drop of 49.5%. The airfoil counts are 23 first vanes in the first row, 46 first blades in the second row, and 23 second vanes in the third row

This study is focused entirely on the first vane (1V) of the HIT RT. The vane has a turning level of 77° and an exit Mach number of 0.88 at mid-span. To create the vane, a set of airfoil profiles were designed at root-, mid-, and tip radii, and these were stacked radially to define the 3D geometry. Additionally, splines were fitted to values of airfoil profile inputs [9], and these were

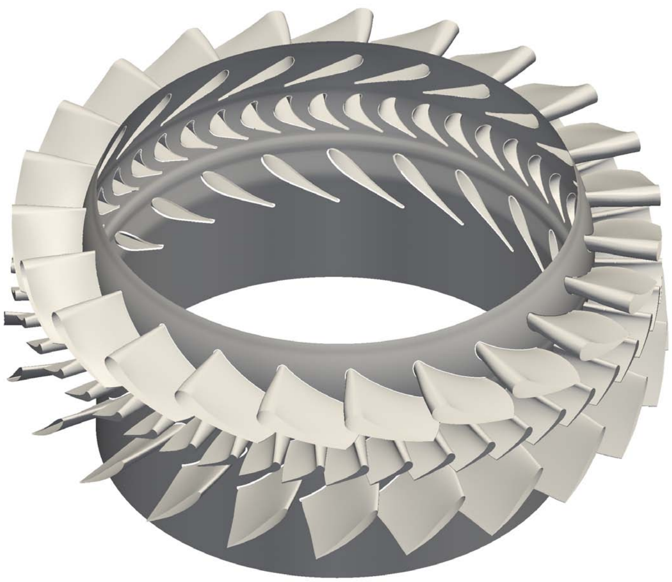

FIGURE 1. AFRL High Impact Technologies Research Turbine (HIT RT)

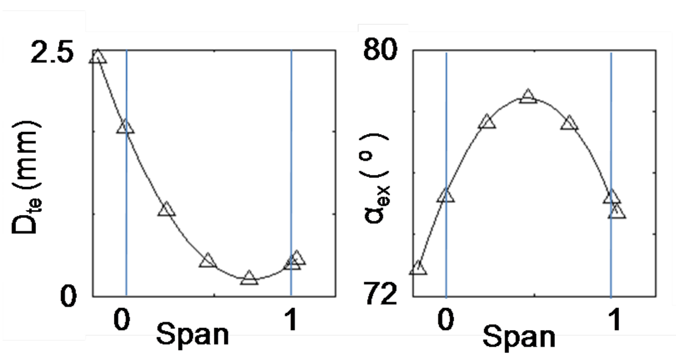

FIGURE 2. Representative spline fits to profile design parameters that were used to define 3D airfoils.

used to define 25% and 75% airfoil sections as well as to create extrapolated airfoil sections that extend the 3D geometry through the endwalls. An example of two such splined profile parameter variations is shown in figure 2. The parameters shown in figure 2 are the airfoil trailing edge diameter, Dte and the airfoil exit angle, α_{ex}. In this way, smooth 3D profiles were assured, and this also aided in 3D grid generation for subsequent unsteady RANS analysis. 3D design features were built into the vane through stacking. It is well known that secondary losses increase with levels of turning through airfoil rows [10]. So, it was decided to design the root and tip profiles with 2° of under-turning and the midspan section with an equal amount of over-turning. Then, the 2D profiles were stacked on the airfoil leading edges. This, combined with the splined airfoil design parameters, resulted in a crescent-shaped trailing edge for the vane itself and an approximately parabolic variation of exit angle out of the airfoil row. It is possible to discern the crescent shape in the former by inspection of figure 3, while the latter is readily apparent in figure 2. The addition of the crescent-shaped trailing-edge feature to the 1V resulted in a 16% reduction in predicted row loss over what was achieved by designing to meanline turning levels alone.

The HIT RT first vane, as seen in figure 3, is a film cooled vane with 648 film cooling holes in total. It consists of an internal cooling passage with six rows of laidback fan-shaped holes on the airfoil pressure side, three rows of laidback fan-shaped holes on the airfoil suction side, six rows of radially angled showerhead holes at the airfoil leading edge, one row of cylindrical holes at the airfoil trailing edge (Figure 4), four rows of laidback fan-shaped holes and one row of cylindrical holes on the hub (ID) platform, and five rows of laidback fan-shaped holes and one row of cylindrical holes on the shroud (OD) platform. The laidback fan-shaped holes have an injection angle of 30°, and diffuse 10° laterally and 10° in the injection plane towards the airfoil surface [11]. The airfoil showerhead holes have a 90° compound angle towards the mid-span and a 30° injection angle.

Figure 4 shows a two-dimensional representation of the film hole layout, however the actual three-dimensional configuration has adjacent rows staggered in the spanwise direction as seen in Figure 3.

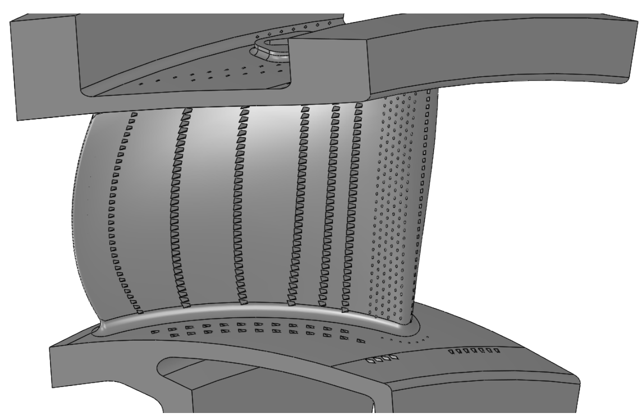

FIGURE 3. Pressure side of the HIT RT first vane showing the staggered nature of the film holes.

To enable the direct validation of durability designs, HIT RT is fully instrumented with double-sided heat flux gages and

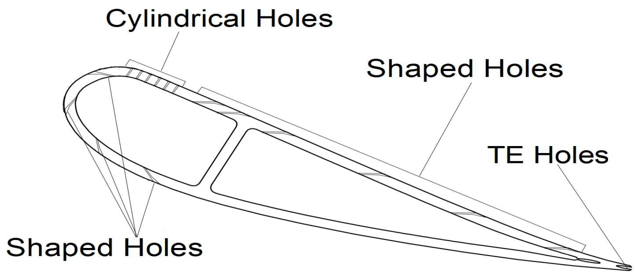

FIGURE 4. Cross section of vane airfoil showing cooling hole row locations. Film holes are staggered in the spanwise direction.

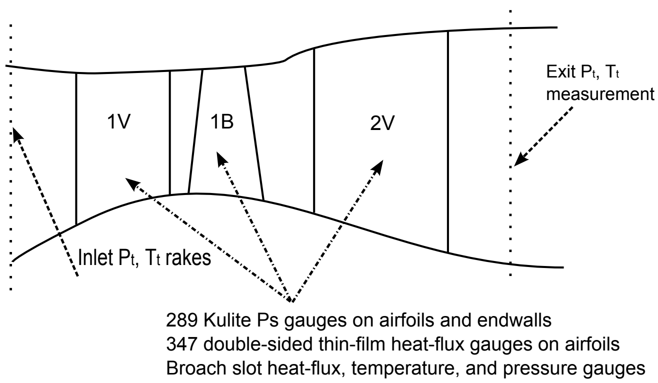

FIGURE 5. HIT RT instrumentation

buried thermocouples for both cooled and uncooled airfoils present in each row. The instrumentation of the HIT RT rig is summarized in figure 5. Experimental data is being acquired and will be available near first quarter of 2011. The numerical results presented here are pre-test predictions of the thermal field on the film cooled first turbine vane.

CHT ANALYSIS METHODOLOGY

A five step conjugate heat transfer analysis procedure was employed in this study:

- Vane and air solid definition
- Mesh generation for both fluid and metal parts
- Boundary and initial condition definition
- Conjugate analysis
- Post-processing and analysis

Vane and Air Solid Definition The incoming CAD geometry is modified from a manufacturing definition to a truly periodic definition with an angular size corresponding to an integer number of airfoils. The modified CAD definition of the airfoil metal solid is then imported into a mesh generation package (e.g. ICEM) so that an air solid may be created around it. CAD features are then grouped based on location and topology for boundary condition assignment and mesh control later in the process.

Generation of Fluid and Solid Mesh Given the complexity of the film cooled turbine vane-including a complex interior structure of the airfoil, internal cooling passages with showerheads and shaped film cooling holes-an unstructured mesh was selected so that the total mesh elements needed to cover all the flow features is within reasonable limits.

With the CAD definition of the vane solid and fluid part obtained from step 1, a tetrahedron mesh with point to point matching at the fluid/solid interface is first created using an octree approach. Laplace volume smoothing is then applied to improve tetrahedron quality before an extrusion layer is created to capture boundary layer effects. Mesh size is controlled by a combination of local geometry curvature and local mesh size specification. Periodic and fluid/solid interface boundaries are meshed with matching nodes. A single extrusion layer is split into multiple layers to capture boundary layer effects on the fluid side, and to improve heat flux predictions near the fluid/solid interface in the solid.

The meshing process automatically provides point-to-point correspondence between nodes located on the fluid/solid interface thus avoiding interpolation of variables across the interface, boundary faces are also tagged with unique names so that boundary conditions can be imposed. Designer productivity is also enhanced with a script to automate the mesh generation procedure for a film cooled vane.

Figure 6 shows the resulting mesh for both solid and fluid parts required for CHT analysis. The enlargement shown in the upper right hand side of the figure depicts the mesh around leading edge shower head and shaped hole. This mesh, used during the development of the CHT process, contained a total of 12 million elements: 4 million for the metal part and 8 million for the fluid.

Boundary and Initial Condition Definition Given a mesh with tagged boundary faces, the solid and fluid parts are initialized and appropriate boundary conditions are imposed at the inlet, exit and attachment points of the solid part. Depending on the mesh size and execution environment, the mesh may be partitioned for parallel execution.

The fluid and solid are both set to $T_t = 305.5K$ with the fluid also having $P_t = 689.5kPa$ and an initial inlet $M = 0.08$. At the turbine exit, a static pressure of $P_s = 358.5kPa$ is initially set at

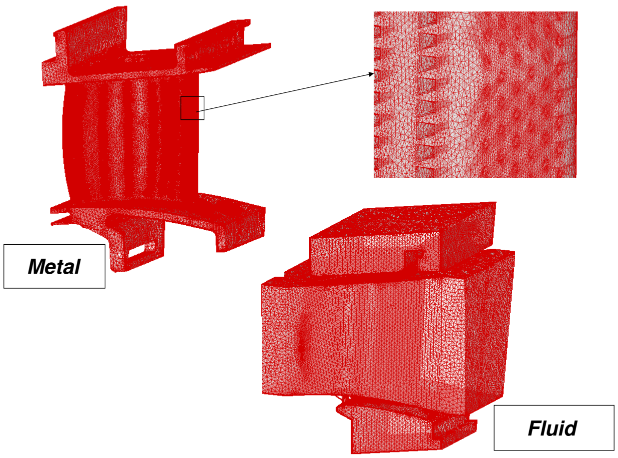

FIGURE 6. Solid and Fluid Mesh for HIT RT first vane

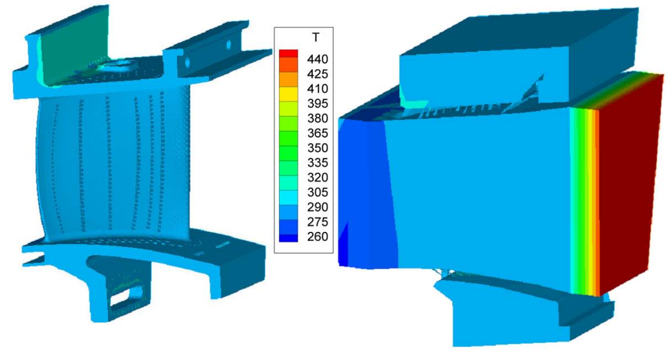

FIGURE 7. Initial and boundary conditions used for the CHT analysis of HIT RT first vane with metal solid on left and fluid on right

the exit boundary. The static pressure initialization varies linearly from the inlet to the exit.

The boundary condition at the inlet of the core flow is held at $P_t = 689.5kPa$, while the total temperature is applied as a step change from the initial conditions with $T_t = 444.4K$.The flow at the inlet is uniform across the inlet and enters in the purely axial direction.The ID and OD cooling flow inlets are set to $P_t = 703.3kPa$, and $T_t = 305.5K$ with radially out and radially in flow vectors respectively. All inlet conditions hold the given total pressure, total temperature, and incoming flow direction. At turbine exit, a radial equilibrium condition with an average pressure of $P_s = 358.5kPa$ is applied at the exit boundary condition.

The metal solid has isothermal boundary conditions on the external faces on the ID and OD surfaces at $T = 305.5K$ and adiabatic conditions on all other external, not fluid/solid interface, boundaries. The solid and fluid domains after applying initial and boundary conditions can be seen in Figure 7.

Numerical experiments have shown that the solution converges faster if one sets the initial fluid temperature for the entire domain to the coolant temperature with a step increase in total temperature at the upstream boundary of the core flow. This is because the cooling fluid is flowing at a very low speed inside the front and rear cavities of the vane as compared with the core flow, thus, it takes a larger computational effort for cold air to reach the film holes if the flow is initialized with a high temperature.

Conjugate Analysis The coupled simulation is then carried out using the Code Leo, to be described in the following section. CHT analysis can be conducted in serial or parallel using support utilities to break up the mesh into multiple blocks suitable for parallel execution.

Post-Processing and Analysis Upon completion of the conjugate analysis, normal post-processing and analysis can be undertaken. Post-processing for this study employed both Tecplot and ParaView in conjunction with the results from the simulation.

Numerical Methods in Code LEO

There are two solver modules in Code Leo: one is used to solve the unsteady Reynolds Averaged Navier-Stokes Equations for fluid flow, while the other is utilized to solve the unsteady heat conduction equation for the prediction of temperature distribution throughout the metal parts.

Flow Solver

Developed by AeroDynamic Solutions, Inc. (ADS), Code Leo employs a cell vertex-centered, finite volume approximation for efficient and accurate modeling of conservation laws of mass, momentum and energy [12] [13]. For each control volume, the Divergence Theorem is used to determine the first derivative of flow properties and a distribution formula was employed to compute the second derivatives for each node defining the volume to determine the shear stresses and heat flux. A distribution formula is also used to provide second order time accurate approximation of the governing equations to determine the changes in flow properties at each node due to convection and propagation. Code Leo is a density-based code and the solution is advanced in time using an explicit time marching scheme. It is second order accurate in space and time.

A two equation $k-\omega$ turbulence model from Wilcox 98 [14] is incorporated in the code which can support both wall function or wall integration. Table lookup is used for modeling ideal gases with variable specific heat ratios. Additionally, the solver utilizes a blend of 2nd and 4th order smoothing to reduce oscillation of the flow field due to shocks and other transient effects.

To speed up convergence rate and reduce computational effort, both a multi-grid scheme for structured mesh and a residual propagation scheme for unstructured mesh are available in Code Leo. For low speed flow problems, preconditioning is also utilized to speed up convergence and provide better numerical accuracy.

For time accurate simulations, Code Leo employs a dual time-stepping method [15] to achieve fast convergence for viscous flow simulation with fine mesh near walls.

There are a number of important capabilities such as, a mixing plane model for steady multistage flow problems, sliding mesh for time accurate simulation with blade/vane interaction, and 2D-non-reflective boundary conditions for cascade flow which have been implemented into code Leo to facilitate the application to turbomachinery flow problems.

Heat Conduction Solver

The heat conduction module was initially developed as a part of an SBIR Phase I grant. Again, the Divergence Theorem and distribution formula are utilized to compute the first and second derivatives of the temperature respectively to get the rate of change in temperature at each node. This approach is first order accurate in time and second order accurate in space. The solution is obtained through a time-marching scheme. A multigrid or residual propagation scheme is used for rapid convergence. Dual-time stepping is also implemented for time accurate heat conduction computations.

To address temperature-dependent material properties on the heat conduction calculation, a linear fit method of properties as function of temperature was incorporated into the heat conduction module so that the effect due to temperature-varying heat capacity and thermal conductivities could be accounted for. Temperature dependent properties are included for nine alloys commonly employed in turbomachinery; other materials may be added easily through a definition file.

Both solvers can be executed efficiently and simultaneously in parallel using standard MPICH2 from Argonne National Labs.

Fluid/Solid Coupling

For conjugate heat transfer, an additional step was added to assure balance in heat flux through the fluid/solid interface.

During each numerical simulation, Code Leo updates fluid properties and metal temperature at each node for both fluid and solid computational domains except for the nodes lying on the interface between fluid and solid. For the nodes on the fluid/solid interface, heat flux values, q, on both sides are also identified and collected. The solution for fluid and the solid is coupled by summing heat flux values q from both the solid and fluid sides

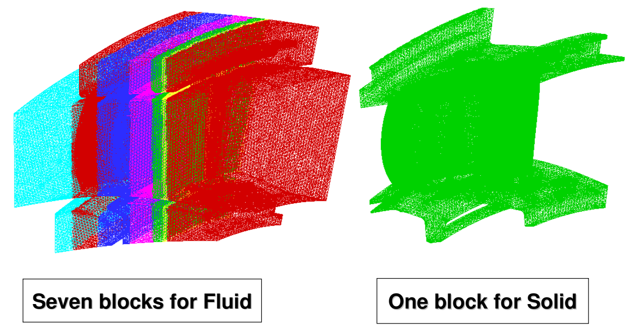

FIGURE 8. Mesh breakup for improved performance.

for nodes at the interface to form the total heat flux:

$$q_{total} = q_{fluid} + q_{solid} \tag{1}$$

The new surface temperature for the solid side, T_s, is then computed using the combined heat flux, q_{total}. T_s is then used to impose the wall temperature T_{wall} on the fluid side.

This process repeats itself for each iteration until the simulation converges when q_{total} at all interface nodes reaches zero.

Parallel Computation

To speed turnaround time, the computational mesh was broken into multiple blocks to support parallel execution.

For this case, the mesh was divided in to eight blocks for execution on a dual quad core machine (Figure 8). One block was assigned to one core for the heat conduction computation of the solid, while the remaining seven blocks, cut axially, were for the fluid simulation. Point to point matching, periodic boundary conditions and the coupling procedure between fluid and solid were executed in parallel. Figure 9 shows the pressure distribution at a constant radial cut for alternate blocks as well as for all blocks to ensure parallel computations were implemented properly.

Solution Convergence

Using the initial mesh, a preliminary calculation was conducted to determine the iterations required for solution convergence. The flow rate, total pressure and total temperature convergence plots resulting from this run are shown in Figure 10.

As can be seen from the figure, inlet and exit flow converged around 15,000 iterations. The predicted flow rate, per airfoil pas-

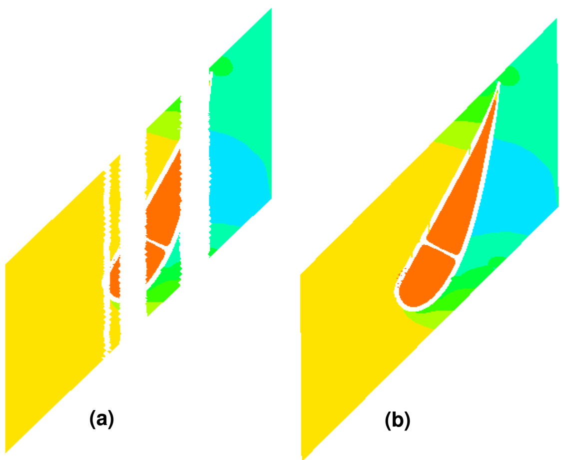

FIGURE 9. Contour plot of static pressure at constant radius. (a) Every other block plotted (b) All blocks plotted.

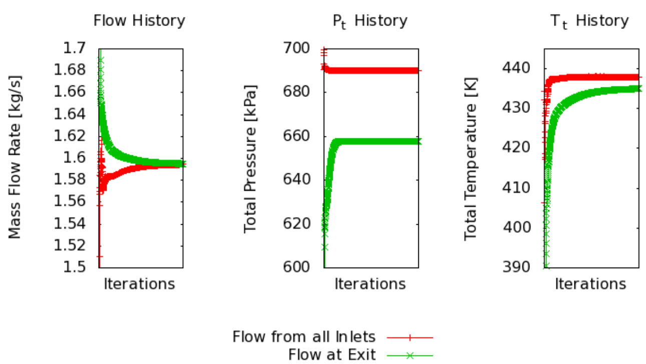

FIGURE 10. Convergence history plots.

sage, was 1.59 kg/s at the exit. Total pressure reached a constant value at a similar number of iterations, reflecting a total pressure loss of 4.5% through the film cooled turbine. It is also interesting to observe that the total temperature showed different values between the inlet and exit due to the constant temperature boundary condition imposed at the attachments.

These results were obtained from a computational mesh consisting of 12 million elements, with 8 million elements in the fluid flow region. A wall function was used for the calculations and the y+ values were 25-40 near the wall surface. Solution convergence was achieved in approximately 50 hours on a dual socket E5504 workstation.

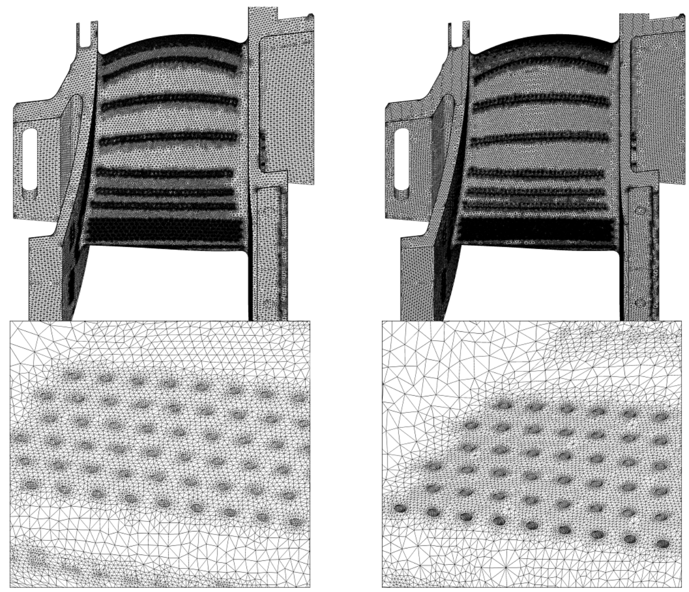

FIGURE 11. Base [left] and fine [right] grained mesh for HIT RT first vane

Mesh Refinement

A mesh refinement study was then conducted to verify the numerical accuracy of the CHT analysis. Two additional meshes were generated:

- A base mesh consisting of 14 million elements (5 million solid, 9 million fluid)
- A fine mesh consisting of 24 million elements (8 million solid, 16 million fluid)

These meshes are shown in Figure 11, along with a close up view around the root section of the leading edge showerhead holes. From the figure, it can be seen that the fine mesh provides better resolution around leading edge film holes and the fillet between the airfoil and endwall. However, there are a few coarse elements embedded in the fine mesh where the curvature is low such as on the shaped hole surfaces. This is due to the choice of using curvature-based mesh refinement in the ICEM meshing process. Numerical results obtained did not reveal anomalies around these coarse areas.

Figure 12 compares the convergence of total temperatures at inlet and exit for the base and fine meshes. It is interesting to note that the inlet and exit mass averaged total temperatures observe the same rate of convergence for both meshes, signifying that the computational effort required for convergence is linearly proportional to the number of elements. The computational time for the fine mesh was 100 hours on the same workstation.

While the mesh refinement study suggested that the base mesh was sufficient to provide reliable prediction of the pressure

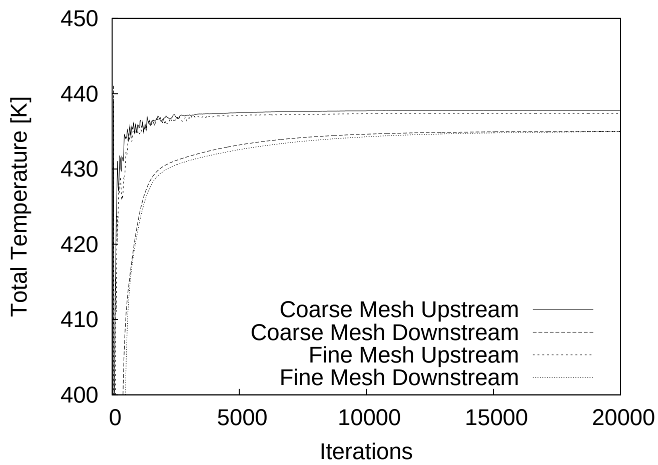

FIGURE 12. T_t convergence plots for base and fine mesh

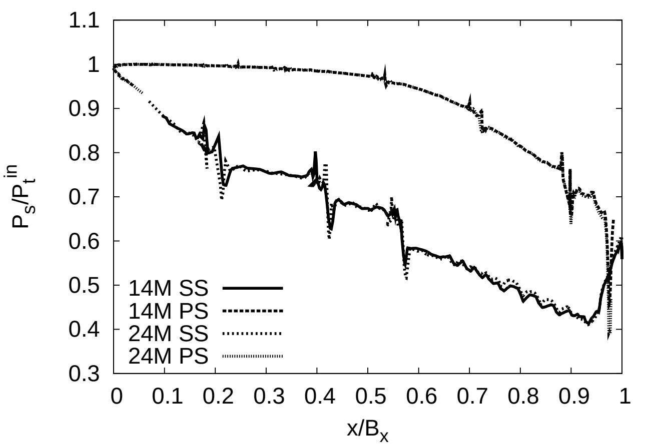

FIGURE 13. Comparison of static pressure distribution at midspan for fine and coarse meshes.

around the airfoil, as seen in Figure 13, an in depth interrogation of the flow field and metal temperature distribution revealed high temperature regions behind several film holes in the coarse mesh solution while the finer mesh did not show this behavior. In addition, it is found that the predicted cooling flow rates, as a percentage of core inlet mass flow rate, with the imposed coolant flow conditions are 4.9% for the coarse mesh and 5.2% for the fine mesh. This shows that the finer mesh results in less numerical blockage of the coolant flow through the film holes. For the discussion in the following section, the results from the fine mesh are presented.

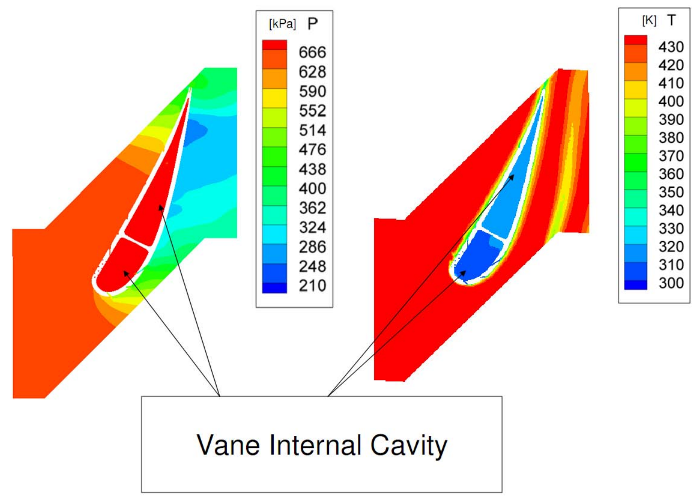

FIGURE 14. Pressure (P_s) and temperature (T_t) contours near mid-span

Results and Discussion

In this section, a number of contour and line plots will be analyzed to provide evidence that the numerical solution obtained is meaningful and provides physical insight from the CHT analysis on the film cooled turbine vane. The contour plots will start with the fluid field first, consisting of pressure and temperature distribution and streamlines, then move to predicted metal temperature distribution on the external of the vane and inside the cavities of the vane.

Figure 14 shows the computed static pressure contour and total temperature contour near mid-span. High static pressure and low total temperature exist in both the front and rear cavities of the vane. From the static pressure contour, high pressure is observed at the inlet as well as rapid reduction of the pressure around the leading edge suction surface, with flow exiting the turbine vane at a low exit pressure corresponding to sonic flow conditions.

The circumferential variation of the exit static pressure is the result of applying a 2D non-reflective boundary condition at exit plane in additional to radial equilibrium condition. This non-reflective boundary results in more realistic flow solutions for exit boundaries located close to the trailing edge plane.

The total temperature contour in Figure 14 shows that the high inlet temperature is convected downstream to the exit plane where there is a layer of lower temperature fluid surrounding the airfoil due to film cooling and the conduction from the cold metal. This layer of cooled fluid also convects downstream along the vane wake and leaves the computational domain.

The total temperature contours at five radial locations are shown in Figure 15, together with streamlines seeded from the inner side of the ID endwall and outer side of the OD endwall

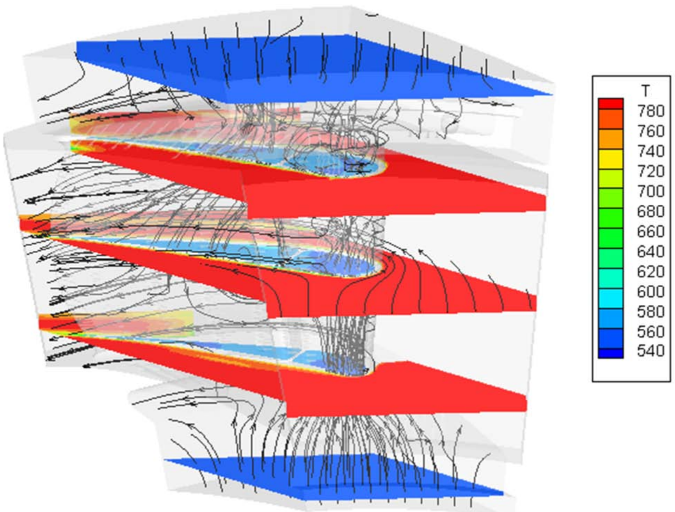

FIGURE 15. Streamline plot depicting cooled air distribution into the vane passage

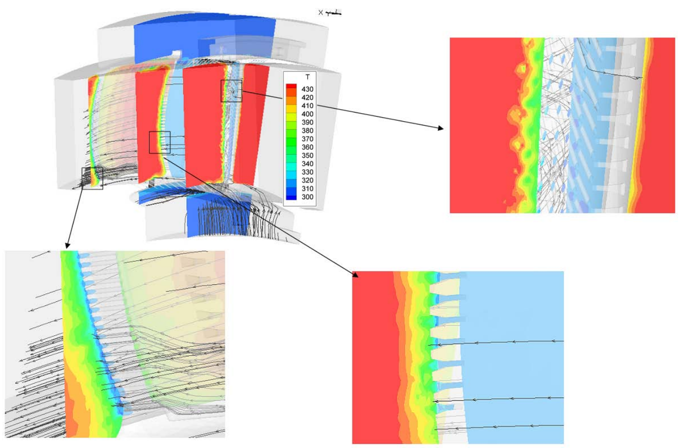

FIGURE 16. Streamline plot of the cooled air passing through the film holes into the main flow passage

to highlight the flow of cooling air . As can be seen, the cooled air in the front cavity of the vane is supplied from the ID side while the cooled air inside the rear cavity comes from the OD side. The cooled air then enters the turbine flow passage through the leading edge shower head holes, the shaped holes on both pressure and suction sides of the vane, and the circular holes at the trailing edge.

Figure 16 provides additional insight on the flow around the cooling holes. It gives total temperature contour plots at three axial cuts across the fluid domain: one axial cut (top right) shows the flow near the leading edge, another at mid-chord (bottom right), and a final cut at the trailing edge of the vane (bottom left).

The upper right hand corner of the figure shows an enlargement of the flow field near the leading edge. The portion of the contours shown in white represents the cut through the metal, while light blue represents the cold air inside the front cavity as well as the flow through the leading edge shower head. The green color represents the cooler air next to the metal surface with a layer of yellow color separating the red-colored external hot gas. Note that the cooling air from the discrete shower heads persists into the core flow region. This is a result of the circular holes having a 30° injection angle without fanning of the holes.

The lower right corner of Figure 16 is the close up view of the flow near shaped holes. Here again, white represents the metal part, blue the cooling air inside the cavity, and red the external hot gas. As can be seen, the segregation of cold and hot is more gradual from the shaped holes than that from the leading edge shower head holes. The dark lines on the plot represent the streaklines coming from the cooling hole upstream.

The lower left side of Figure 16 shows a close up of the flow field near the root of the trailing edge. It shows cooling air leaking through the trailing edge circular holes. The large spread of the cold layer shown in the figure is mainly due to the axial cut through the flow field with a very steep flow angle.

To verify the proper coupling of fluid and solid temperature predictions, an investigation of the temperature field near the leading edge mid-span was conducted.

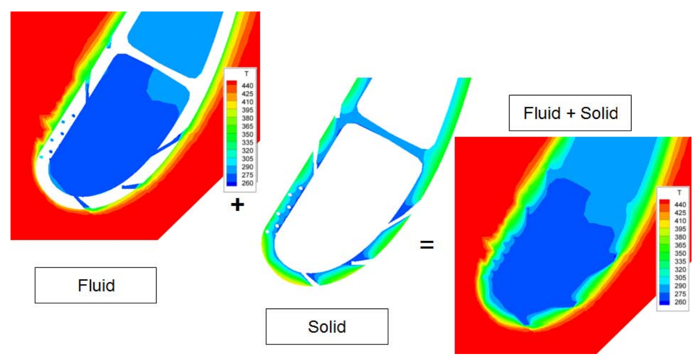

FIGURE 17. Temperature field near leading edge near mid-span

Figure 17 shows the fluid-only, solid-only and composite views of the temperature field. The fluid-only contour shows the cold flow inside the front cavity as well as the cold flow leaking through the film cooling holes. A layer of low temperature fluid surrounds the external side of the turbine vane. The solid-only temperature contour can be seen in the middle of Figure 17. It properly shows lower temperature on the inside of the cavity and

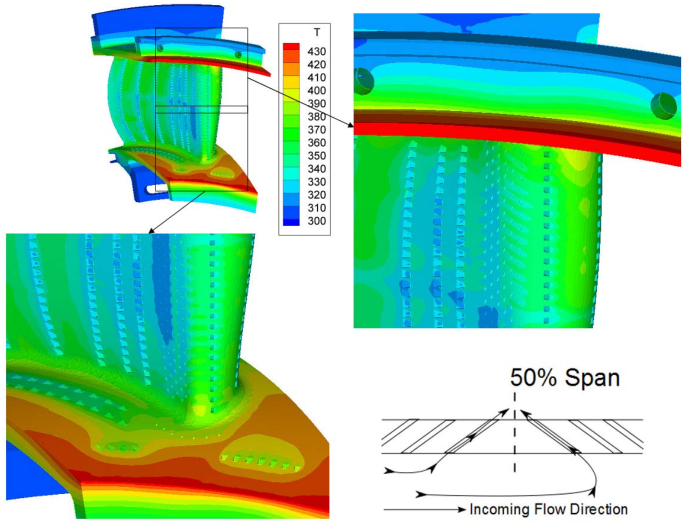

FIGURE 18. Predicted pressure side metal temperature

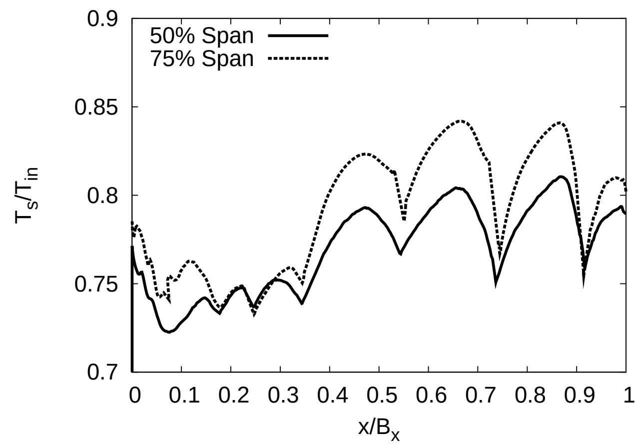

FIGURE 19. Predicted pressure side metal temperature

higher metal temperature for the metal exposed to the hot external gas.

The composite temperature contour for both fluid and solid is given on the right side of Figure 17. The continuous temperature field between fluid and solid implies that the coupling procedure has been implemented properly.

The predicted surface metal temperature for the HIT RT vane was then investigated. The predicted surface metal temperature for the pressure side can be seen in Figure 18, along with close ups for two sections.

The lower left portion of Figure 18 provides a close up view of the temperature distribution on the inner diameter platform. It properly shows lower metal temperature behind the film holes on the ID endwall. The upper right hand of Figure 18 provides a close up view of the metal temperature around the leading edge shower head and the shaped holes downstream of the leading edge.

As expected, the metal temperature is lower behind the holes. Closer examination of the map indicates that the core flow is stagnating between the third and fourth rows of the leading edge shower head holes. There is a strip of cold region along the mid-span section of the vane. This is due to the large amount of cold air piling up in the region where the leading edge shower heads point toward each other as shown in the lower right corner of Figure 18. This pile up corroborates with the recent research from Johnson et. al. on a flat plate with similar film hole placement [11]. An asymmetry can be seen in the surface temperature distribution around the leading edge shower head holes in Figure 18. This was not seen in the experimental results from Johnson et. al. but in that case the coolant was fed from a direction normal to the plate whereas in the actual airfoil the coolant is fed radially outward, which means that the cooling flow must turn at least 150° in order to exit the showerhead holes past the midspan.

In Figure 19 a plot of surface temperature at the midspan and 75% span demonstrates that the coolant builds up along at the midspan resulting in lower temperatures. Additionally, it can be seen that the highest temperature following a film cooling row occurs not immediately before the following row, as expected from classical moethods predictions, but between half and three quarters of the way between the rows. This suggests that the heat conduction through the solid due to the film cooling holes has a strong effect on the surface temperature upstream of the hole.

Figure 20 provides the total temperature contour plot at six axial locations. The lower left plot is the total temperature contour for an axial plane in front of the vane leading edge. The hot gas from the inlet is shown in red, the cooling flow in blue, and the warm layer next to the airfoil external surface in green. As can be seen, the cold air around mid span is spreading out into the external hot gas region. On the same figure, five more axial cuts are provided starting from the leading edge and moving toward the vane trailing edge in the counter-clockwise direction. It can be seen that the high concentration of cooled air persists along the mid-span location until the trailing edge. It is observed from additional simulations that the concentration depends strongly on the supply pressure of the cooling air.

Figure 21 provides the metal temperature distribution on the ID and OD platforms, as well as the inside front and rear cavities of the film cooled vane. It shows that the metal temperature is lower around the cooling holes due to the cold fluid passing through. It also shows that higher metal temperature around the corners inside the cavity due to slow flow circulation.

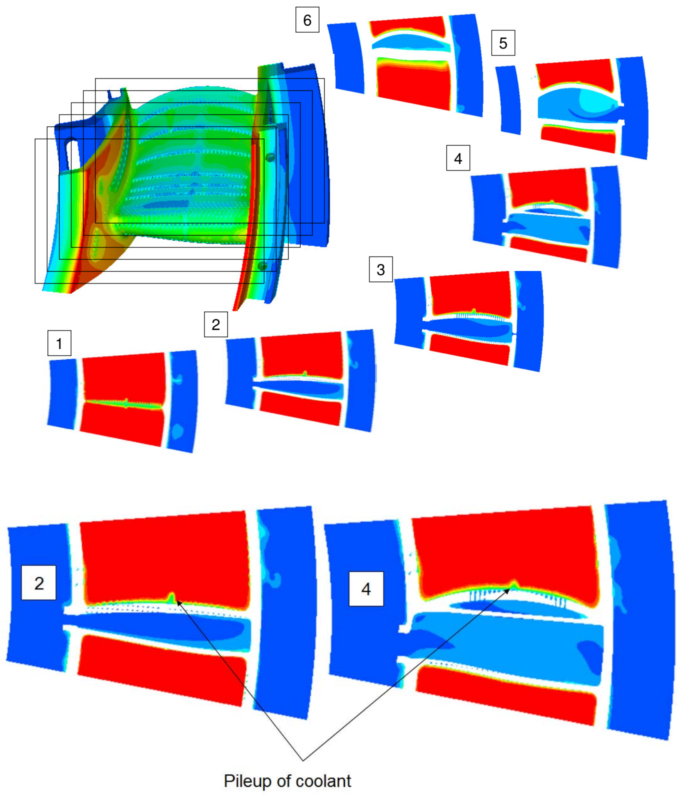

FIGURE 20. Top: Cooled air behavior on pressure surface at midspan. Bottom: Closeup view of coolant pileup on pressure surface.

Conclusion

In summary, conjugate heat transfer analysis for the HIT RT film cooled turbine vane was conducted successfully. An unstructured mesh with prism layers was generated for both fluid and solid parts using ICEM, with point to point matching at the fluid/solid interface to avoid interpolation errors. Simulations were carried out using the base and fine mesh with Code LEO and the results from the fine mesh were presented in detail. The solution was shown to make physical sense and provide additional insight into the interaction between the fluid and solid. The computational time for a mesh having 24 million elements was shown to be 100 hours using a dual-socket Intel E5504 workstation. The combination of meaningful flow insights and fast turnaround time resulting from this CHT simulation procedure will allow engineers to assess its accuracy and advantages against a wide variety of turbine configurations.

As a second phase of this project, we will compare predictions against experimental data.

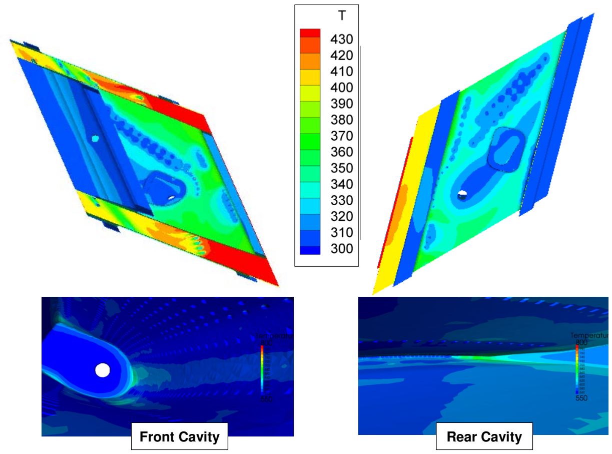

FIGURE 21. Predicted metal temperatures for the ID and OD platforms as well as internal cavities

ACKNOWLEDGMENT

This project was conducted under the support of a United States Air Force SBIR grant.

REFERENCES

[1] Heidmann, J., Rigby, D., and Ameri, A., 2000. "A three-dimensional coupled internal/external simulation of a film-cooled turbine vane". *Journal of Turbomachinery,* ***122***, p. 348.

[2] Rahaim, C., and Cavalleri, R., 1996. "Coupled finite volume and boundary element analysis of conjugate heat transfer problems". In AIAA, Thermophysics Conference, 31 st, New Orleans, LA.

[3] Guo-Tai, L., and Chi, W., 2003. "NUMERICAL SIMULATION METHOD OF AERODYNAMICS-THEMODYNAMICS COUPLING IN 3-D TURBINE CASCADE [J]". *Journal of Engineering Thermophysics,* ***5***.

[4] Bohn, D., Bonhoff, B., and Schoenenborn, H., 1995. "Combined aerodynamic and thermal analysis of a high-pressure turbine nozzle guide vane". In Yokohama International Gas Turbine Congress, Yokohama, Japan; JAPAN; 22-27 Oct, Tokyo, Japan: Gas Turbine Society of Japan.

[5] York, W., and Leylek, J., 2003. "Three-dimensional conjugate heat transfer simulation of an internally-cooled gas turbine vane". ASME.

[6] He, L., and Oldfield, M., 2009. "Unsteady Conjugate Heat Transfer Modelling". ASME.

[7] Clark, J., Polanka, M., Meininger, M., and Praisner, T.,

2006. “Validation of Heat-Flux Predictions on the Outer Air Seal of a Transonic Turbine Blade”. *Journal of Turbomachinery,* ***128***, p. 589.

[8] Praisner, T., Grover, E., Knezevici, D., Popovic, I., Sjolander, S., Clark, J., and Sondergaard, R., 2008. “Toward the expansion of low-pressure-turbine airfoil design space”. ASME.

[9] Clark, J., Koch, P., Ooten, M., Johnson, J., Dagg, J., McQuilling, M., Huber, F., and Johnson, P., 2009. Design of Turbine Components to Answer Research Questions in Unsteady Aerodynamics and Heat Transfer. Tech. rep., Tech. Rep. AFRL-RZ-WP-TR-2009-2180, AFRL.

[10] Benner, M., Sjolander, S., and Moustapha, S., 2006. “An empirical prediction method for secondary losses in turbinespart I: a new loss breakdown scheme and penetration depth correlation”. *Journal of Turbomachinery,* ***128***, p. 273.

[11] Johnson, J. e. a., 2010. “Infrared Assessment of Overall Effectiveness of a Modern Turbine Vane Cooling Scheme”. In AIAA 2010-7126.

[12] Ni, R., 1981. “A multiple grid scheme for solving the Euler equations”. In In: Computational Fluid Dynamics Conference, 5th, Palo Alto, Calif., June 22, 23, 1981, Collection of Technical Papers.(A81-37526 16-34) New York, American Institute of Aeronautics and Astronautics, Inc., 1981, p. 257-264., Vol. 1, pp. 257–264.

[13] Ni, R., 1989. “Prediction of 3 D multi-stage turbine flow field using a multiple-grid Euler solver”. In AIAA, Aerospace Sciences Meeting, 27 th, Reno, NV, p. 1989.

[14] Wilcox, D. C., 2003. *Turbulence Modeling for CFD, Second Edition*. DCW Industries, Inc.

[15] Davis, R., Shang, T., Buteau, J., and Ni, R., 1996. “Prediction of 3-D unsteady flow in multi-stage turbomachinery using an implicit dual time-step approach”. In AIAA, ASME, SAE, and ASEE, Joint Propulsion Conference and Exhibit, 32 nd, Lake Buena Vista, FL.